INSTITUTE OF PHYSICS PUBLISHING NETWORK: COMPUTATION IN NEURAL SYSTEMS

Network: Comput. Neural Syst. **14** (2003) 647–672 PII: S0954-898X(03)57706-5

High-frequency, depressing inhibition facilitates synchronization in globally inhibitory networks

S Kunec[1] **and A Bose**[2,3]

[1] Center for BioDynamics, Boston University, Boston, MA 02215, USA
[2] Department of Mathematical Sciences, New Jersey Institute of Technology, Newark, NJ 07102, USA
[3] Courant Institute of Mathematical Sciences, New York University, New York, NY 10012, USA

E-mail: kunec@bu.edu and bose@njit.edu

Received 19 December 2002, accepted for publication 26 June 2003
Published 1 August 2003
Online at stacks.iop.org/Network/14/647

Abstract

Motivated by the study of sharp wave-associated ripples, high-frequency (∼200 Hz) extracellular field oscillations observed in the CA1 region of the rat hippocampus during slow-wave sleep and periods of behavioural immobility, we consider a single inhibitory neuron synapsing onto a network of uncoupled, excitatory neurons. The inhibitory synapse is depressing and has a small synaptic delay. Each excitatory cell provides instantaneous, positive feedback to the inhibitory cell. We show that the interneuron can rapidly synchronize the action potentials of the pyramidal cells if the frequency of inhibitory input is increased in a ramp-like manner as occurs during the ripple. We show that the basin of attraction of the synchronous solution is larger when the inhibition frequency is gradually increased as opposed to remaining constant.

1. Introduction

Although the brain contains a huge number of neurons and synapses, its size is nonetheless finite. For this simple reason, it is important that a given network of neurons within the brain has the ability to display a multitude of rhythmic behaviours across different behavioural states. It is of great interest to understand not only the variety of stable patterns the network exhibits, but also how the network transitions between these states.

Several prior modelling studies have identified potential mechanisms responsible for different rhythms in a variety of contexts. This includes work on transitions between spindle and delta rhythms in the thalamus [17, 21], on synchronization at beta and gamma frequencies in the hippocampus [11] and on transitions between low- and high-frequency oscillations due to synaptic depression in the crustacean STG [1, 15], to name only a few. A primary goal of all of these studies is to show which intrinsic or synaptic mechanisms could be functionally relevant in determining behaviour of the neuronal network in question.

In this work, we are interested in the role of interneurons in shaping activity patterns in a model network loosely based on the CA1 region of the hippocampus. Buzsaki and co-workers have empirically observed in the hippocampus of rats that during moments of behavioural immobility, consummatory activities and slow-wave sleep, the CA1 region exhibits what is known as the sharp wave-associated ripple (SPWR) [2, 26]. The SPWR is caused by a concentrated wave of excitation called the sharp wave (SPW). The SPW originates in the CA3 region of the hippocampus, where a portion of the pyramidal cell network synchronizes for 40–120 ms. The SPWs occur with a frequency anywhere from 0.02 to 3 Hz.

The primary excitatory output of the CA3 region is along the Schaffer collaterals to the CA1 region. During the SPW event, the CA3 pyramidal cell network synchronizes sending a concentrated pulse of excitation to both the pyramidal cells and the interneurons of the CA1 region, where the SPWR is observed. The ripple is a high-frequency (200 Hz) extracellular field oscillation which is characterized by relatively low-frequency, but synchronous, firing of a small subset of CA1 pyramidal cells, and high-frequency (presumably synchronous) activity of a larger set of CA1 interneurons. Some of these interneurons have been shown to oscillate at around 200 Hz for the duration of the ripple wave [26]. In the time interval between SPWs (and associated ripples), excitation from CA3 to CA1 is low and pyramidal cells in CA1 fire intermittently and non-synchronously, while interneurons tend to also fire with low frequency.

The SPWR is of interest for several reasons. Among them, the CA1 network organizes and displays synchronous activity in a short amount of time, within a few milliseconds [26], implying that intrinsic and synaptic mechanisms used to produce these results may operate on the same time scale. Also, it has been suggested that SPWRs play an important role in memory consolidation and transfer of memories from the hippocampus to the entorhinal cortex. During exploratory behaviour, the CA3 region of the rat hippocampus displays an extracellular oscillation in the theta frequency range, as the animal receives new information. During this time, groups of excitatory, pyramidal cells may strengthen their mutual, recurrent collaterals, forming assemblies, through synaptic modification [9]. When the rat sleeps or becomes immobile, these groupings synchronize, producing the SPWs that cause SPWRs in the CA1 region. Any pyramidal cells that fire concurrently with the SPW excitation are thought to have a powerful impact on 'downstream' (posthippocampal) targets [26].

As suggested by the evidence above, the SPWR is a network phenomenon. In contrast to CA3, CA1 pyramidal cells have a relatively sparse recurrent collateral system [3], but make a number of synaptic connections to a variety of interneurons. Interneurons, on the other hand, make a large number of connections on one another and also onto target pyramidal cells [24]. Given the possible absence or low probability of direct pyramidal cell to pyramidal cell connections in CA1, the basic question arises of how these cells synchronize during the ripple. At least two credible theories have been put forth concerning this phenomenon: excitation from CA3 propagates through pyramidal cell axo-axonal gap junctions to promote synchrony [5, 23, 25]; or pyramidal cells and interneurons interact through particular feedback mechanisms to foster synchrony [26].

This paper promotes the second ideology. We show how ramping up the frequency of inhibition and synaptic depression can be used to synchronize action potentials of uncoupled pyramidal cells. We consider two uncoupled pyramidal cells which make excitatory synapses onto a single interneuron (the PIP network; see figure 1). The interneuron sends a reciprocal depressing inhibitory synapse onto each of the pyramidal cells.

We pay particular attention to the role of depression in the synchronization of pyramidal cells as interneuron frequency increases. High frequency inhibition effectively suppresses pyramidal cell firing as well as synchronizing them below threshold. Depression of the inhibitory synapses allows the pyramidal cells to eventually fire as the synaptic conductance

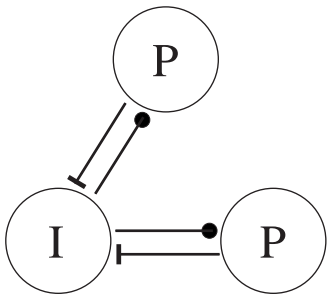

Figure 1. The PIP sub-network. The sub-network consists of one inhibitory cell (I) and two excitatory cells (P). The inhibitory cell synapses onto both P cells, while both P cells synapse onto the I cell. The inhibitory synapse is depressing and contains a small, synaptic delay. The excitatory connections are non-depressing and are instantaneous.

decreases over time. This mechanism of subthreshold synchronization is robust in the presence of pyramidal cell heterogeneity.

The outline of the paper is follows. In section 2, our main results are described. In section 3, we present the model equations for each cell as well as the assumptions utilized in order to employ techniques of geometric singular perturbation theory. Section 4 presents the analysis which underlies our results. Section 5 more fully explores the effects of the simulation parameters on the simulation results. Finally, in section 6, we discuss the implications of our results and compare them with other work.

2. Results

The main focus of this paper is to present a process by which the simple PIP network synchronizes its pyramidal cells. This serves to suggest a mechanism whereby the actual CA1 network rapidly organizes it excitatory components. Depressing, inhibitory synapses are the key mechanisms of this operation.

In figures 2–4, we show three simulations which illustrate the main point of this paper. All simulations were started with the same initial conditions for the P cells. In figure 2 the inhibition frequency is $\sim$200 Hz, in figure 3 the frequency is $\sim$23 Hz and in figure 4 the frequency is ramped between these two values over a 30 ms window starting at $t = 400$ ms. Notice that in the first two figures the pyramidal cells do not synchronize, but instead tend to an out-of-phase solution. In the latter, however, the pyramidal cells synchronously fire. In fact, the synchronization seems to occur very rapidly in the sense that the first spike fired by both cells after the increase in inhibition frequency is already synchronized.

At high inhibitory frequencies, repeated, rapid use of the synapse lowers its effectiveness, allowing the cells to be essentially uncoupled. At low inhibitory frequencies, the synapse is able to recover and maintain its strength. In this case, the strong inhibition serves to drive the cells apart, but is not renewed quickly enough to suppress their firing.

However, by varying the inhibitory frequency from low to high, the initial repetitive inhibition suppresses pyramidal cell firing, synchronizing them below threshold, while the depression eventually allows the cells to fire together synchronously, as seen in figure 4. The rest of this paper is devoted to analytically establishing and explaining the results shown in figures 2–4.

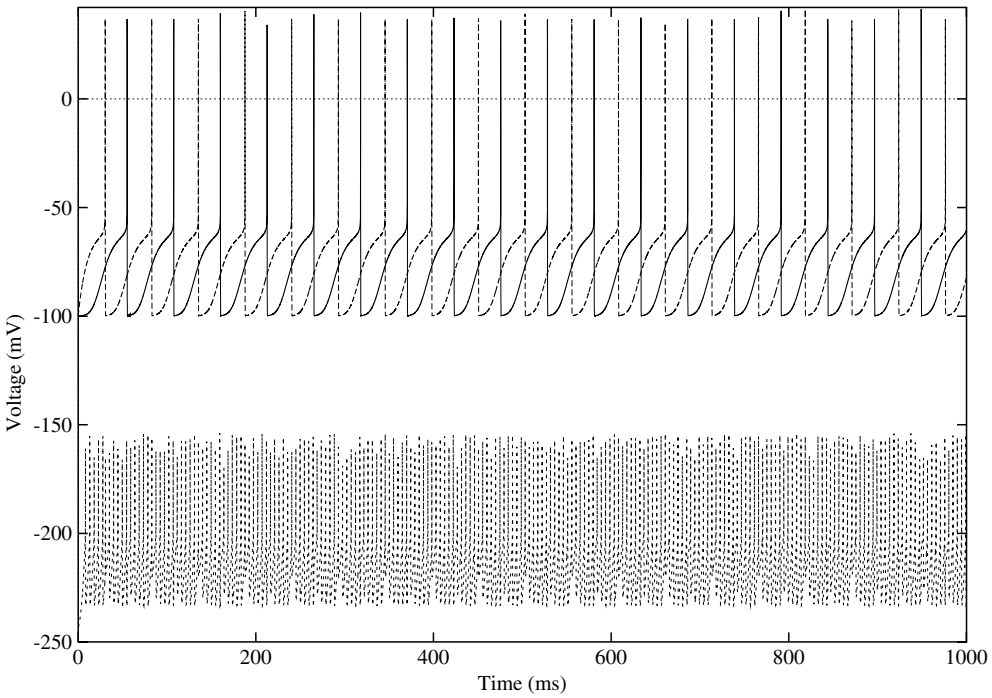

Figure 2. High-frequency, depressing inhibition loses its effectiveness at steady state, allowing the pyramidal cells to oscillate asynchronously. The P cells started at initial conditions $v_{p1} = v_{p2} = -100$ mV, $w_{p1} = 0.9$ and $w_{p2} = 0.1$. The I cell started at $v_{i1} = -100$ mV and $w_{i1} = 0.9$. The level of depressing, inhibitory, synaptic resources, D_1 and D_2, were initially set to 0 to simulate high-frequency use at steady state. The inhibition has a synaptic delay of 1 ms. The I cell oscillated at ∼200 Hz. The I cell is offset by 150 mV.

3. The model

In this section, we describe the equations used to model pyramidal cells and interneurons, and the synapses between them. Later, we will list assumptions that help simplify the analysis of the equations.

3.1. Individual neurons

Both excitatory and inhibitory neurons are characterized as relaxation oscillators. In general, such a neuron adheres to the following general set of equations:

$$\begin{aligned} \frac{\mathrm{d}v}{\mathrm{d}t} &= f(v, w) \\ \frac{\mathrm{d}w}{\mathrm{d}t} &= \epsilon\left[\frac{w_\infty(v) - w}{\tau_w(v)}\right], \end{aligned} \tag{1}$$

where $\epsilon \ll 1$ is a singular perturbation parameter. The nonlinearity f contains various ionic currents which are intrinsic to the cell. The nonlinearity $w_\infty - w$ controls the opening and closing of a potassium channel associated with the cell.

The nullclines of (1) are found by setting the right-hand side equal to zero. The geometric shape and the relative position of the system's nullclines in the phase plane are important to the

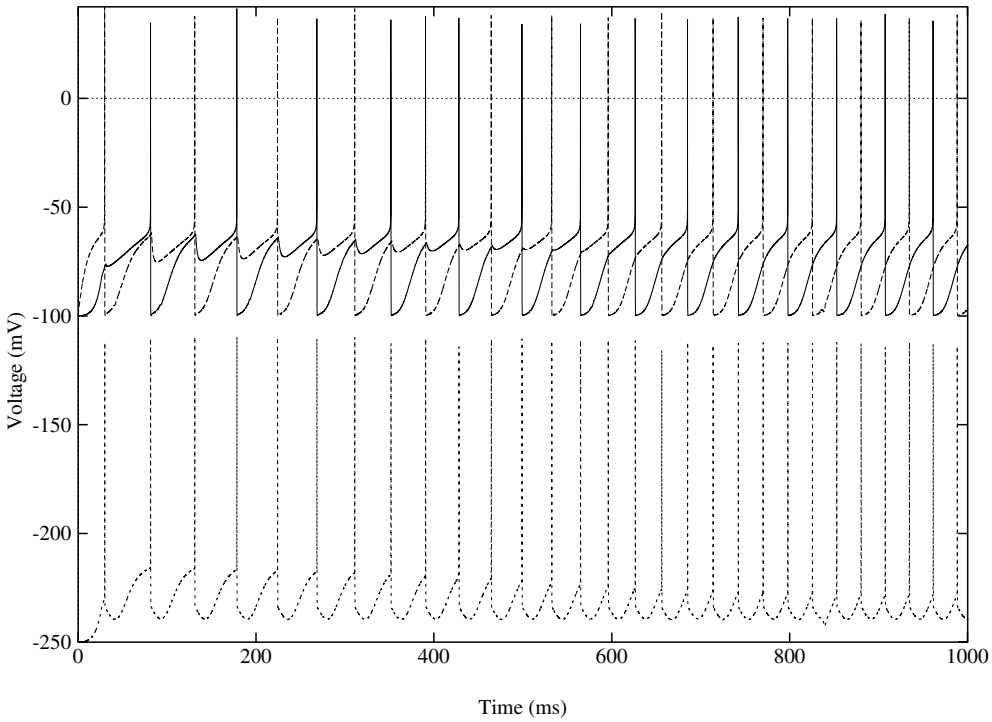

Figure 3. Low-frequency, depressing inhibition maintains its effectiveness at steady state, pushing the pyramidal cell into anti-phase. The P cells started at initial conditions $v_{p1} = v_{p2} = -100$ mV, $w_{p1} = 0.9$ and $w_{p2} = 0.1$. The I cell started at $v_{i1} = -100$ mV and $w_{i1} = 0.9$. The level of depressing, inhibitory, synaptic resources, D_1 and D_2, were initially set to 1 to simulate low-frequency use at steady state. The inhibition has a synaptic delay of 1 ms. The I cell oscillated at ∼23 Hz. The I cell is offset by 150 mV.

analysis presented later. The v-nullcline is a cubic-shaped curve $\mathcal{C}_0 = \{(v, w) : f(v, w) = 0\}$. We let $p_{lk} \equiv (v_{p_{lk}}, w_{p_{lk}})$ denote the local minimum (also called the left knee) of $\mathcal{C}_0$ and $p_{rk} \equiv (v_{p_{rk}}, w_{p_{rk}})$ denote the local maximum (the right knee) of $\mathcal{C}_0$. The w-nullcline is a non-decreasing sigmoid, $\mathcal{S} = \{(v, w) : w_\infty - w = 0\}$.

The functions f and $w_\infty - w$ satisfy the following requirements: $f > 0$ ($f < 0$) below (above) $\mathcal{C}_0$, and $w_\infty > w$ ($w_\infty < w$) below (above) $\mathcal{S}$. Near the left branch of $f = 0$, we require that $f_w < 0$ and $f_v \neq 0$ at all points except the minimum of the cubic. We assume that $\mathcal{S}$ intersects $\mathcal{C}_0$ at only one point. If this intersection lies on the middle branch of $\mathcal{C}_0$, this critical point is unstable, allowing the cell to oscillate. If this intersection lies on either the right or left branch of $\mathcal{C}_0$, then the critical point is stable and globally attracting.

For ϵ sufficiently small, (1) possesses a stable periodic solution provided that its critical point lies on the middle branch. We exploit the smallness of ϵ to formally construct this solution. Letting $\epsilon \to 0$ in (1), we obtain the fast reduced system:

$$\begin{aligned} \frac{\mathrm{d}v}{\mathrm{d}t} &= f(v, w) \\ \frac{\mathrm{d}w}{\mathrm{d}t} &= 0. \end{aligned} \tag{2}$$

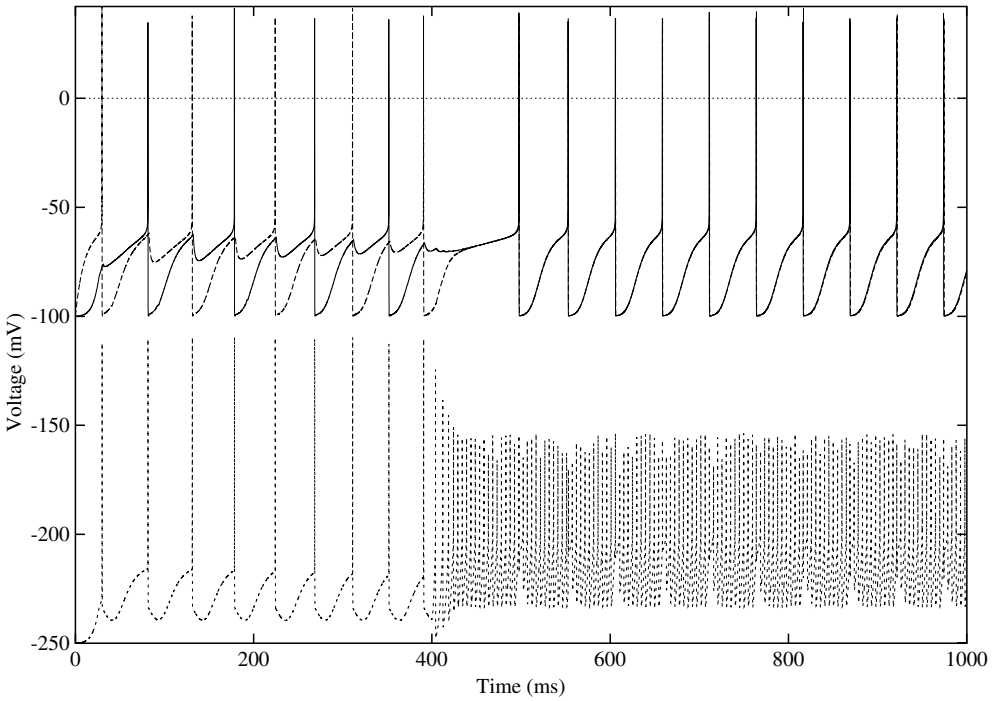

Figure 4. A ramp-like increase of inhibition frequency synchronizes the pyramidal cells. The P cells started at initial conditions $v_{p1} = v_{p2} = -100$ mV, $w_{p1} = 0.9$ and $w_{p2} = 0.1$. The I cell started at $v_{i1} = -100$ mV and $w_{i1} = 0.9$. The level of depressing, inhibitory, synaptic resources, D_1 and D_2, were initially set to 1 to simulate initial levels of resources. The inhibition has a synaptic delay of 1 ms. The increase of current starts at $t = 400$ ms and reaches a maximum 30 ms later, where it remains. This causes the I cell to increase its frequency from ∼23 to ∼200 Hz. The I cell is offset by 150 mV.

Re-scaling time by $\tau = \epsilon t$ and then letting $\epsilon \to 0$ yields the slow reduced equations:

$$\begin{aligned} 0 &= f(v, w) \\ w' &= \frac{w_\infty(v) - w}{\tau_w(v)}, \end{aligned} \tag{3}$$

where $' \equiv \frac{\mathrm{d}}{\mathrm{d}\tau}$. A singular periodic orbit consisting of four pieces, two slow pieces (solutions of (3)) and two fast transitions (solutions to (2) between the slow pieces) is shown in figure 5. The fast transitions are initiated from the left and right knees of $\mathcal{C}_0$. For ϵ sufficiently small, the actual periodic orbit lies close to the singular solution just described [13].

3.2. Synapses and the resulting network equations

Neurons communicate at synapses, whereby the 'transmitting' or pre-synaptic cell sends a synaptic current to the 'receiving' or post-synaptic cell, causing either an increase or a decrease in the voltage of the latter cell. If such a connection is present, the voltage equation is modified to be

$$\frac{\mathrm{d}v}{\mathrm{d}t} = f(v, w) - \bar{g}_{\mathrm{syn}} s(t - \tau_d)[v - E_{\mathrm{syn}}], \tag{4}$$

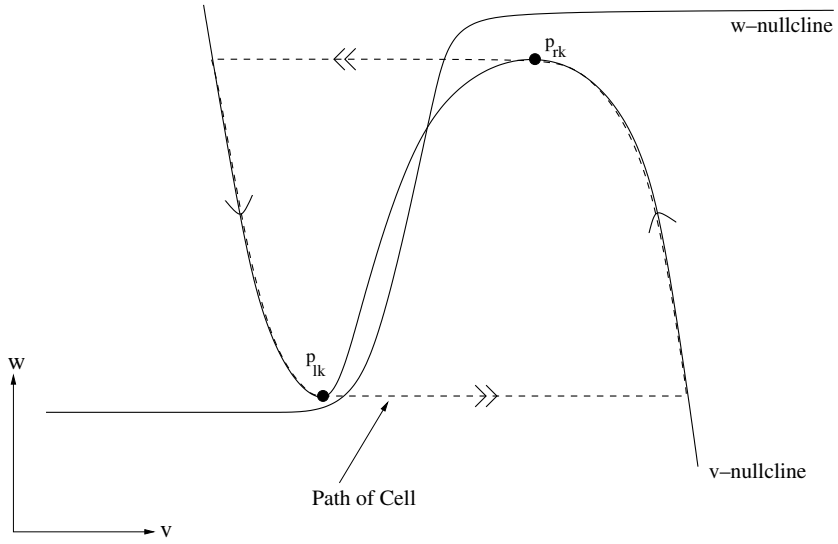

Figure 5. Oscillatory cell's trajectory in the v–w phase plane.

where the variable s is the synapse's effective strength and the parameters $\bar{g}_{\rm syn}$ and $E_{\rm syn}$ are the maximum synaptic conductance and the synapse's reversal potential, respectively; the subscript syn = exc or inh for excitatory or inhibitory synapses, respectively. The parameter τ_d is the synaptic delay.

The value of $E_{\rm syn}$ determines whether the synapse is excitatory ($E_{\rm exc} = 0$ mV) or inhibitory ($E_{\rm inh} = -80$ mV). When activated, excitatory (inhibitory) synapses tend to raise (lower) $\mathcal{C}_0$ in the v–w phase plane. If $\bar{g}_{\rm syn}s$ is not too large, then the ensuing nullcline given by $f(v, w) - \bar{g}_{\rm syn}s(t - \tau_d)[v - E_{\rm syn}] = 0$ is still cubic shaped.

In our model, the synapse from each P to I is excitatory and non-depressing. There is no synaptic delay in these synapses. The I to P synapses are inhibitory, depressing and subject to a non-zero conduction delay τ_d. For the excitatory synapses, we use a standard model given by

$$\frac{{\rm d}s}{{\rm d}t} = \frac{[1-s]}{\tau_1} H_\infty(v_{\rm pre} - v_\theta) - \frac{s}{\tau_2} H_\infty(v_\theta - v_{\rm pre}), \tag{5}$$

where $v_{\rm pre}$ denotes the voltage of a pre-synaptic pyramidal cell; H_∞ is the Heaviside function with threshold v_θ; the values τ_1 and τ_2 are time constants of rise and decay of the synapse. Both are O(1) with respect to ϵ. We shall say that a neuron is in its active state if it is above threshold and in its silent state if it is below.

We model the depressing, inhibitory synapses as in [1]. A variable D measures the level of depression of the synapse and evolves independently of s. In this model, the variable s is set equal to D whenever the presynaptic interneuron is above threshold. The equations are

$$\begin{aligned} \frac{{\rm d}D}{{\rm d}t} &= \frac{\epsilon[1-D]}{\tau_a} H(v_\theta - v_{\rm pre}) - \frac{\epsilon D}{\tau_b} H(v_{\rm pre} - v_\theta) \\ \frac{{\rm d}s}{{\rm d}t} &= \frac{D-s}{\tau_g} H(v_{\rm pre} - v_\theta) - \frac{\epsilon s}{\tau_k} H(v_\theta - v_{\rm pre}). \end{aligned} \tag{6}$$

The variable s represents the synapse's effective strength. The variable D represents the 'resources' of the synapse, such as the amount of neurotransmitters available to the synapse.

The parameter τ_k is the time constant governing the decay of the effective strength of the inhibiting synapse while below synaptic threshold and τ_a controls the rate of D's recovery while below synaptic threshold. The parameter τ_b is the time constant in control of the use of these 'synaptic resources' while the presynaptic cell is above the synaptic threshold. The time constant τ_g determines the rate at which the synaptic strength matches the synaptic resources, i.e. the synaptic rise time. Note that while the above equations for the synapses are discontinuous due to the presence of the Heaviside functions, there is no difficulty in smoothing these out. Our use of the Heaviside is for mathematical simplicity.

The presence of ϵ in various places in (6) implies that D evolves on the slow time scale at all moments in time, while s evolves on the slow time scale when the interneuron is below threshold. When it is above threshold, s approaches D on the fast time scale, but then evolves with D. Thus when the interneuron is above threshold, (6) reduces to

$$\begin{aligned} D' &= \frac{-D}{\tau_b} \\ s &\equiv D. \end{aligned} \tag{7}$$

When the interneuron is below threshold, (6) reduces to

$$\begin{aligned} D' &= \frac{1-D}{\tau_a} \\ s' &= \frac{-s}{\tau_k}. \end{aligned} \tag{8}$$

If the interneuron oscillates with a constant period, the synaptic resources lost and regained during each cycle will balance and s will approach a steady-state oscillation.

3.3. Simplifying assumptions

We now list some assumptions which will simplify the analysis. An additional assumption is made near the end of the next section.

- **(A1)** All action potentials of pyramidal cells and interneurons are thin and of fixed duration T_{spike}. The time T_{spike} is small compared to T_{in} (the intrinsic time the I cell spends in the silent state) and the intrinsic time that the P cell spends in the silent state. This can be achieved by making $\tau_w(v)$ small on the right branch compared to the left branch.
- **(A2)** The time T_{spike} is small compared to τ_d (the inhibitory synaptic delay). For spiking models, this assumption may be reasonable. In our simulations, the width of any action potential is less than 1 ms and the synaptic delay is 1 ms.
- **(A3)** The I cell has a refractory period longer than the synaptic delay τ_d. Outside of this refractory period, any time that a pyramidal cell fires, I also fires.
- **(A4)** For P cells in the silent state, the functions $w_\infty(v) = 0$ and $\tau_w(v) = \tau_w$ is constant.
- **(A5)** We only consider the $\epsilon = 0$ reduced equations to construct singular periodic solutions. The work in [13] can be used to show that for ϵ sufficiently small, there exists an actual period orbit which is $O(\epsilon)$ close to the singular one.

3.4. The w–g phase plane

Because of the above assumptions, the dynamics of the entire system can be understood by focusing on the behaviour of the P cells while they lie in their silent state. To do so, we define a two-dimensional slow manifold on which the P cells evolve while in the silent state.

Let $g = \bar{g}_{\text{inh}} s$, where g represents the conductance of the inhibitory synapse. When a P cell lies in the silent state, it will follow one of two sets of equations depending on whether or

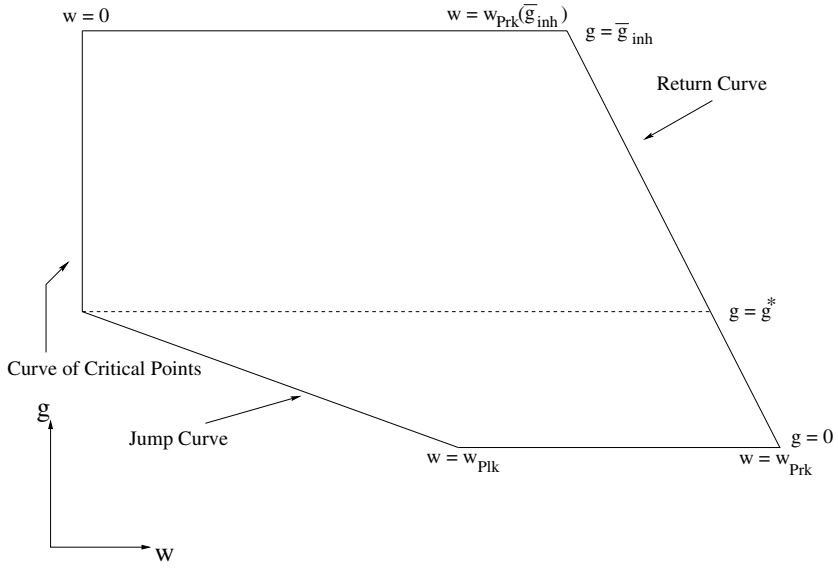

Figure 6. The w–g phase plane.

not the interneuron is silent or active. Assume for a moment that the synaptic delay $\tau_d = 0$ and consider (3), (4), **(A4)**, and (8). When I is silent, each P obeys an equation of the form

$$\begin{aligned} 0 &= f(v, w) - g[v - E_{\text{syn}}] \\ w' &= -w/\tau_w \\ D' &= [1 - D]/\tau_a \\ g' &= -g/\tau_k. \end{aligned} \tag{9}$$

When I is active, we use (7) instead of (8) and the equations are

$$\begin{aligned} 0 &= f(v, w) - g[v - E_{\text{syn}}] \\ w' &= -w/\tau_w \\ D' &= -D/\tau_b \\ g &\equiv \bar{g}_{\text{inh}} D. \end{aligned} \tag{10}$$

If the synaptic delay $\tau_d \neq 0$, then P obeys either of the above equations with a delay τ_d after the interneuron changes state. In both (9) and (10), the first equation is algebraic. Since $f_v \neq 0$ for all points except at the left knees, we can solve this equation for v in terms of w and g. Namely, we define $v = F(w, g)$ whenever P lies in its silent state, where the equation is valid at the left knees by continuity of the flow. The second through fourth equations in (9) and (10) are used to calculated the evolution of w and g, which are then used to determine v. Thus the entire dynamics of P can be tracked on a two-dimensional slow manifold, parametrized by the variables w and g as shown in figure 6. This manifold has five boundary curves: the horizontal lines (1) $g = 0$ and (2) $g = \bar{g}_{\text{inh}}$; (3) the curve of critical points; (4) the jump curve and finally (5) the return curve.

The curve of critical points is defined by the intersection of the sigmoid $\mathcal{S}$ with the left branch of any of the cubics found for different values of g. By assumption **(A4)**, the curve of critical points is defined simply by $w = 0$. However, it exists only for an interval $g \in [g^*, \bar{g}_{\text{inh}}]$ where g^* is the minimum value of g that produces a cubic which intersects $\mathcal{S}$.

The jump curve is defined by the w-position of the minimum of the cubic as g varies, $w_{p_{lk}}(g)$. A pyramidal cell leaves the silent state whenever it reaches the jump curve. The jump curve is negatively sloped in the w–g plane, as shown by the following argument (this calculation here is not new and can be found for example in [22]). Let $\Phi(v, w, g) = f(v, w) - g[v - E_{\text{inh}}]$. Note that $\Phi = 0$ along the w–g slow manifold. The jump curve is characterized by $\Phi_v = 0$. Let $(v_{p_{lk}}(g), w_{p_{lk}}(g))$ denote the position along the jump curve as a function of g. Plugging this into $\Phi = 0$ and differentiating with respect to g, we find

$$0 = \Phi_v \frac{\partial v_{p_{lk}}}{\partial g} + \Phi_w \frac{\partial w_{p_{lk}}}{\partial g} + \Phi_g. \tag{11}$$

Using the jump curve condition that $\Phi_v = 0$ and rearranging terms shows that the slope of the jump curve satisfies

$$\frac{\partial g}{\partial w_{p_{lk}}} = \frac{-\Phi_{w_{p_{lk}}}}{\Phi_g} = \frac{\partial f/\partial w}{v_{p_{lk}}(g) - E_{\text{inh}}}. \tag{12}$$

By the assumption $\partial f/\partial w < 0$, and with E_{inh} chosen to be less than $v_{p_{lk}}$ for any value of g, the above slope is negative. The negativity of this slope will have importance for synchronization, as we show later. We make one final simplification.

(A6) The jump curve on the w–g manifold is linear and has slope equal to $-M$, $M > 0$.

The return curve is defined analogously to the jump curve but instead uses the maximum of the cubic as g varies, $w_{p_{rk}}(g)$. A similar argument to above shows that it is also negatively sloped in the w–g plane. After firing, P cells return to the silent state along the return curve. Figure 7 depicts what the return curve, the jump curve and the curve of fixed points looks like in the v–w phase plane.

4. Analysis of the PIP network

We now demonstrate why ramping the frequency of I promotes synchronization of the P cells. The main goal of this section is to show how T_{in} affects the synaptic conductance g being felt by each P cell, and how this in turn affects the time they spend in the silent state. To this end, in the following, we now consider T_{in} as an independent variable. Recall that T_{in} is the inter-spike interval of I in the absence of any excitatory input, and can be thought of as determining the intrinsic frequency of I.

4.1. Dynamics of a single pyramidal cell in the w–g phase plane

We first describe the behaviour of a single P cell, which is reciprocally connected to I. Suppose the system has reached steady state. The inhibitory conductance will reach a steady-state oscillation with maximum value g_{peak} and minimum value g_{min}. Figure 8 shows a plot of how g_{peak} and g_{min} vary as a function of T_{in}, offset down by an amount equal to g^*. The curves g_{peak} and g_{min} are determined analytically (see appendix A) and are given by

$$g_{\text{peak}} = \begin{cases} \bar{g}_{\text{inh}} \dfrac{1 - \exp(-T_{\text{in}}/\tau_a)}{1 - \exp(-T_{\text{in}}/\tau_a)\exp(-T_{\text{spike}}/\tau_b)} & \text{for } T_{\text{in}} < T_{\text{max}} \\ \bar{g}_{\text{inh}} \dfrac{1 - \exp(-T_{\text{max}}/\tau_a)}{1 - \exp(-T_{\text{max}}/\tau_a)\exp(-T_{\text{spike}}/\tau_b)} & \text{for } T_{\text{in}} \geqslant T_{\text{max}} \end{cases} \tag{13}$$

and

$$g_{\text{min}} = \begin{cases} g_{\text{peak}} \exp(-T_{\text{spike}}/\tau_b)\exp(-T_{\text{in}}/\tau_k) & \text{for } T_{\text{in}} < T_{\text{max}} \\ g_{\text{peak}} \exp(-T_{\text{spike}}/\tau_b)\exp(-T_{\text{max}}/\tau_k) & \text{for } T_{\text{in}} \geqslant T_{\text{max}}. \end{cases} \tag{14}$$

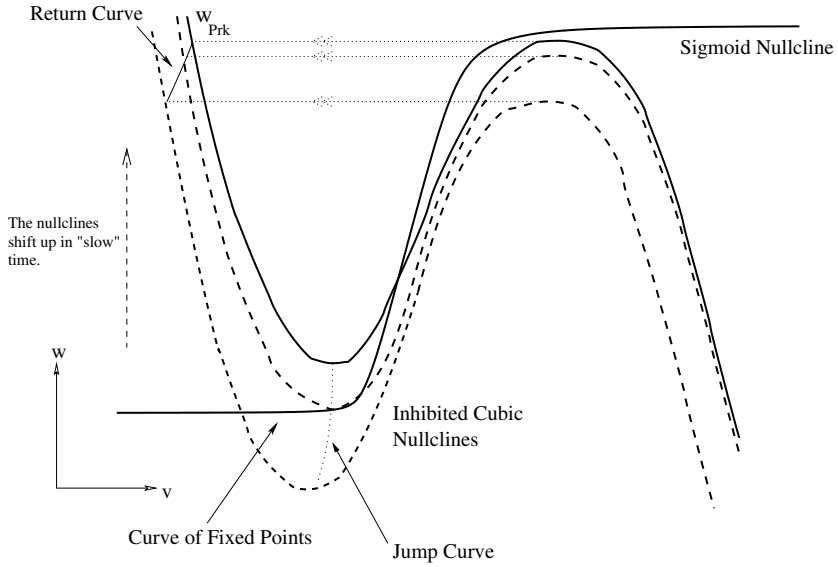

Figure 7. Movement in the v–w phase plane (the effects of inhibition). After receiving inhibition, the cubic nullcline may intersect the sigmoid nullcline on its left branch, producing the stable curve of fixed points. As the inhibition decays, the nullcline shifts up in 'slow' time. P leaves the silent state from the jump curve. P returns from the active state to the left branch of the cubic nullcline, along the return curve. As is seen, each of these curves depends on g.

To understand these formulae, first consider an isolated I cell. Its frequency of spiking is determined by T_{in}, which then determines g_{peak} and g_{min}. When I is reciprocally coupled to P, provided that T_{in} is small enough, then T_{in} still determines g_{peak} and g_{min} because the firing of I is essentially determined by its intrinsic properties. When T_{in} is too big, meaning that the intrinsic frequency of I is small, then I fires whenever P does because of the excitatory synapse. In this case, g_{peak} and g_{min} will be determined by how long P (and consequently I) stays in the silent state. This time turns out to be a constant and is called T_{max}. In appendix A we give a proof of the existence and uniqueness of T_{max}.

When T_{in} is small, g_{peak} is small corresponding to a weak synapse. As T_{in} increases, so does g_{peak}, thus strengthening the synapse. The shape of these curves can be inferred from (13) and (14). Note that to the left of T_{max}, g_{peak} is a monotonically increasing function of T_{in}, while g_{min} has a single local maximum. Using (13),

$$\frac{\mathrm{d}g_{\text{peak}}}{\mathrm{d}T_{\text{in}}} = \bar{g}_{\text{inh}} \frac{\exp(-T_{\text{in}}/\tau_a)[1-\exp(-T_{\text{spike}}/\tau_b)]}{\tau_a[1-\exp(-T_{\text{in}}/\tau_a)\exp(-T_{\text{spike}}/\tau_b)]^2}, \tag{15}$$

it is apparent that $\mathrm{d}g_{\text{peak}}/\mathrm{d}T_{\text{in}} > 0$ for all T_{in}.

To understand the local maximum of g_{min}, we use (14) to find

$$\frac{\mathrm{d}g_{\text{min}}}{\mathrm{d}T_{\text{in}}} = \exp(-T_{\text{spike}}/\tau_b)\exp(-T_{\text{in}}/\tau_k)\left[\frac{\mathrm{d}g_{\text{peak}}}{T_{\text{in}}} - g_{\text{peak}}/\tau_k\right]. \tag{16}$$

Note that the first multiplicative term is strictly positive. For $T_{\text{in}} = 0$, using (15) and that $g_{\text{peak}}(0) = 0$, the second term in (16) is positive. So the slope of the g_{min} curve at the origin is positive. Next observe that the first of the two terms within the brackets decreases to 0, while the second term increases from 0, both as functions of T_{in}. Thus there is a single value of T_{in} at which $\mathrm{d}g_{\text{min}}/\mathrm{d}T_{\text{in}} = 0$. This value is easily seen to correspond to a local maximum.

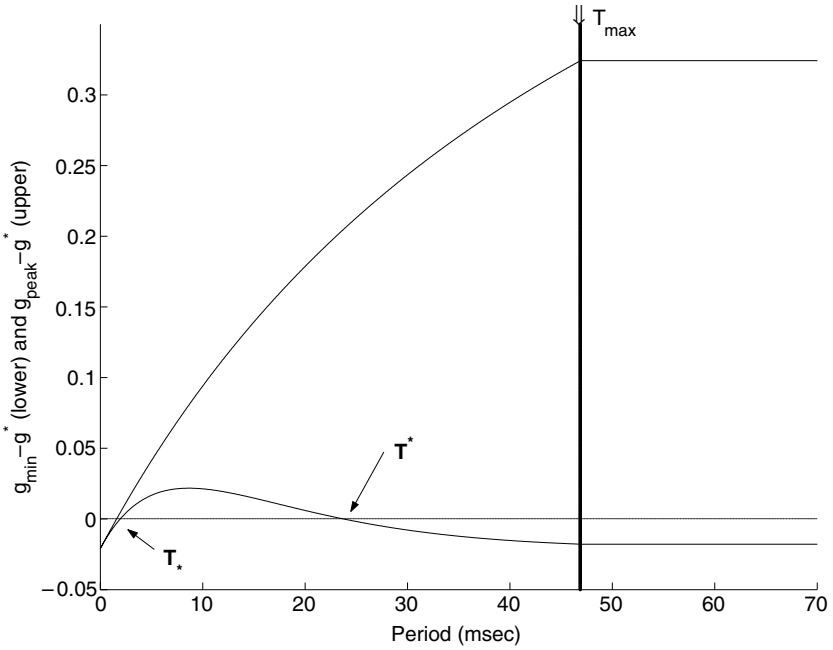

Figure 8. $g_{\min} - g^*$ (lower curve) and $g_{\text{peak}} - g^*$ (upper curve) versus T_{in}. To the left of $T_{\max}$, both curves depend on T_{in}. To the right of $T_{\max}$, both curves achieve constant values. The parameter values used are those listed in appendix B. The following parameters were estimated from simulations: $g^* = 0.021$ ms cm^{-2}, $T_{\max} = 46.9$ ms, and $T_{\text{spike}} = 0.01$ ms.

The single local maximum of $g_{\min}$ reflects the fact that there are two competing effects occurring as T_{in} increases. The value g_{peak} increases with T_{in}, while $\exp(-T_{\text{in}}/\tau_k)$ decreases with T_{in}. The former is primarily controlled by τ_a and τ_b and the latter is primarily controlled by τ_k. The value of $g_{\min}$ at the local maximum is dependent on these parameters, but also depends strongly on $\bar{g}_{\text{inh}}$. Thus it is easy to choose parameters in such a way that the local maximum of $g_{\min}$ lies above g^*. By continuity, this implies that there exist values T_* and T^* such that if $T_{\text{in}} \in [T_*, T^*]$, then $g_{\min} > g^*$. When this is the case, the inhibition from I to P is strong enough and is renewed frequently enough to completely suppress P from firing.

We can use figure 8 to understand how a single P cell evolves in the w–g phase plane. Figure 9 shows the trajectory of the P cell for three different values of T_{in}. Trajectory A occurs when $T_{\text{in}} > T_{\max}$ is so large that I only fires when P does. In this case, the synapse from I to P has a long time to recover, so the initial value of g is large. Since I does not fire until P does, the trajectory of the latter decays monotonically to the jump curve. The time P spends in the silent phase is primarily controlled by the synaptic parameter τ_k, the decay time constant of the inhibitory synapse. Trajectory C occurs when $T_{\text{in}} < T_*$ is very small so that I fires many times for each spike of P. Now the synapse is very weak, so the initial value of g is small. Moreover, with each firing of I, the trajectory of P moves vertically up on the w–g phase plane and then decays. Here the time P spends in the silent phase is primarily controlled by its own intrinsic properties and in particular by τ_w. Trajectory B occurs for intermediate values of $T_{\text{in}} \in [T_*, T^*]$. In this case, the inhibition frequency is initially strong enough ($g > g^*$) and renewed frequently enough to completely suppress P from firing. Thus P spends an infinite amount of time in the silent state.

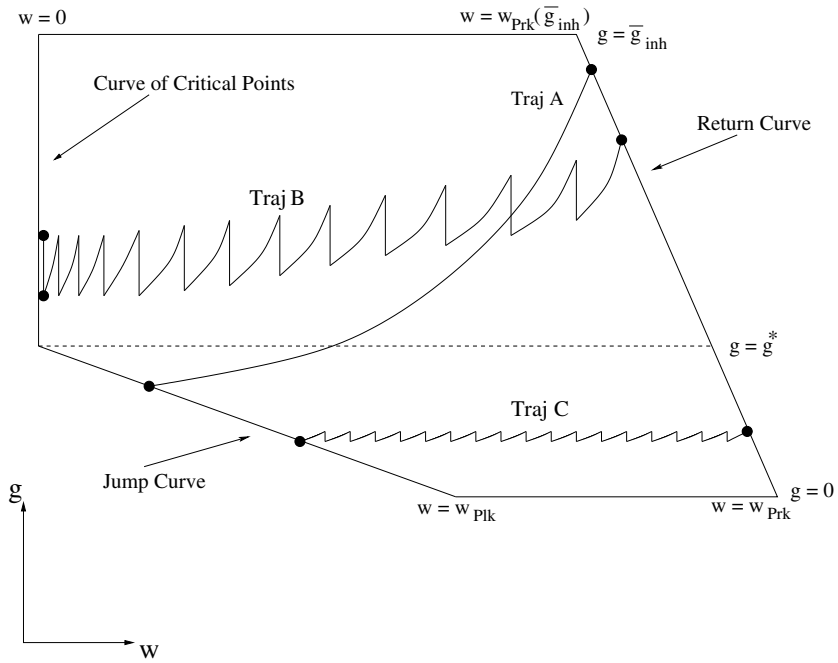

Figure 9. Three sample trajectories in the w–g phase plane. Trajectory A shows how a P cell approaches the jump curve with low-frequency inhibition. The I cell fires only when the P cell fires, and thus the trajectory is monotonic. Trajectory C shows how high-frequency inhibition has little effect on the firing properties of a P cell, since the inhibitory synapse's strength is minimal. Trajectory B shows how certain inhibition frequencies will suppress P cell spikes. The I cell's synapse fires slowly enough to recover its synaptic resources, but fast enough to prevent the synapse from decaying sufficiently to allow the P cell to fire.

4.2. The synchronous solutions

In this section, we establish the existence and stability of synchronous solutions. Proving existence is trivial since the behaviour of each of the P cells in a synchronous solution for a particular value of T_{in} will be identical to the behaviour of a single P cell coupled to I as described in section 4.1. That is, if two cells start out synchronized they stay synchronized. We therefore turn our attention to proving stability of the synchronous solution.

As shown in section 3.4, the slope of the jump curve is negative. This has an important consequence for the P cells as they evolve in the silent state. Consider the two P cells with initial conditions: (w_1, g_0) and (w_2, g_0) with $w_1 < w_2$. Since these cells always have equal g values, and since w evolves independently of g, we define the w-time between cells as the time it takes for the trailing cell's w value to evolve to the position of the leading cell's w value, provided that the leading cell is not already at the jump curve. This time is invariant as the cells evolve along the w–g phase plane. Suppose initially that the w-time between the cells is δt. When the leading cell reaches the jump curve, the w-time will still be δt. Note, however, that because the jump curve has negative slope, the trailing cell will reach the curve of knees with a w value that is greater than the w value of the leading cell when it jumped. When one cell is at the jump curve, we define the w-time to be the time it takes the trailing cell to reach the jump curve. This time is now less than δt. In other words, the negative slope of the jump curve promotes synchronization of the cells provided that the w-time between them is less than τ_d.

However, let us consider the cells as they return from the active phase. Recall that the return curve is also negatively sloped in the w–g phase plane. The slope of this curve can also be calculated using (12) by replacing $v_{p_{lk}}(g)$ with $v_{p_{rk}}(g)$. This negative slope implies that there may actually be an expansion of time between cells on the jump back to the silent state. Since $v_{p_{rk}}(g) > v_{p_{lk}}(g)$, the term $v_{p_{rk}}(g) - E_{\text{inh}}$ may be quite large implying that the slope of the return curve may be much less negative than the slope of the jump curve. When the trailing cell returns to the silent state, a small change in g may produce a large change in w, and the w-distance between the cells may be larger than the previous return. Since we measure our time difference in w-time, the time between the cells may be larger. In other words, if the inhibition decays while the trailing cell is in the active state, the trailing cell could spend *more* time in the active state than the leading cell. If this were the case, then the synchronizing effects achieved in the silent state could be lost during the active state and subsequent return to the silent state.

The potential desynchronization of the cells in the active state can be removed or at least minimized in the following ways. First, the explicit assumptions **(A1)** and **(A2)** imply that both cells spend exactly T_{spike} in the active state. Thus the trailing cell would not spend extra time in the active state, as the inhibition decays. Second, independent of these assumptions, the term $\partial f/\partial w$ typically involves a potassium ionic current (see appendix B or for example other models such as Morris–Lecar [14]). Thus $\partial f/\partial w$ would contain a term involving $v_{p_{rk}}(g) - E_K$ for the return curve and $v_{p_{lk}}(g) - E_K$ for the jump curve. The former is larger than the latter, thus tending to make the slope of the return curve more negative. In particular, this term would also tend to mitigate the effects of E_{inh} on the slope of the curves.

Using **(A1)**, **(A2)** and that the w-time between cells is less than δt at the jump curve, we can now show stability of the synchronous solutions. For synchrony, we need to show that if two cells start a w-time distance δt apart and close to the synchronous solution, then after they fire, they are less than δt apart. The above argument shows that when the cells fire, their w-time is less than δt. By assumptions **(A1)** and **(A2)**, each spends the same amount of time T_{spike} in the active state, and as a result when both cells return to the silent state, their w-time distance is exactly the same as at the moment of the jump. During the spike and ensuing return to the silent state, it is important to remember that both cells receive the same level of inhibition. In the w–g phase plane, this means that the cells lie at the same horizontal g-level and thus their w-time distance apart can easily be measured. In particular, when the trailing cell returns to the silent state, this time is less than δt, thus showing stability of the synchronous solution.

4.3. Basin of attraction

The above proof shows that the negativity of the slope of the jump curve is sufficient to prove stability of the synchronous solution. It does not, however, address what the basin of attraction of the solution may be. Indeed the basin of attraction of the synchronous solution depends strongly on the synaptic delay τ_d. Clearly when one cell is at the jump curve, the other cell needs to be within τ_d of it in w-time to be in the basin of attraction of the synchronous solution. If it is not, then the cells tend to an out-of-phase or anti-phase solution. We do not prove the existence or stability of such solutions here, but see [12] for related results.

To understand whether two initial conditions will synchronize, let us consider again the dynamics along the w–g slow manifold (see figure 10). Consider two cells with initial conditions given by (w_1, g_0), (w_2, g_0), $w_1 < w_2$ and $\Delta w_0 = w_2 - w_1$. Suppose the leading cell (the one starting at (w_1, g_0)) reaches the jump curve after time $t = t_f$ with $g = g_f$. The difference in the w values of the two cells at this time is easily seen to be $\Delta w(t_f) = \Delta w_0 \exp(-t_f/\tau_w)$. The trailing cell will lie on the horizontal line $g = g_f$. We are

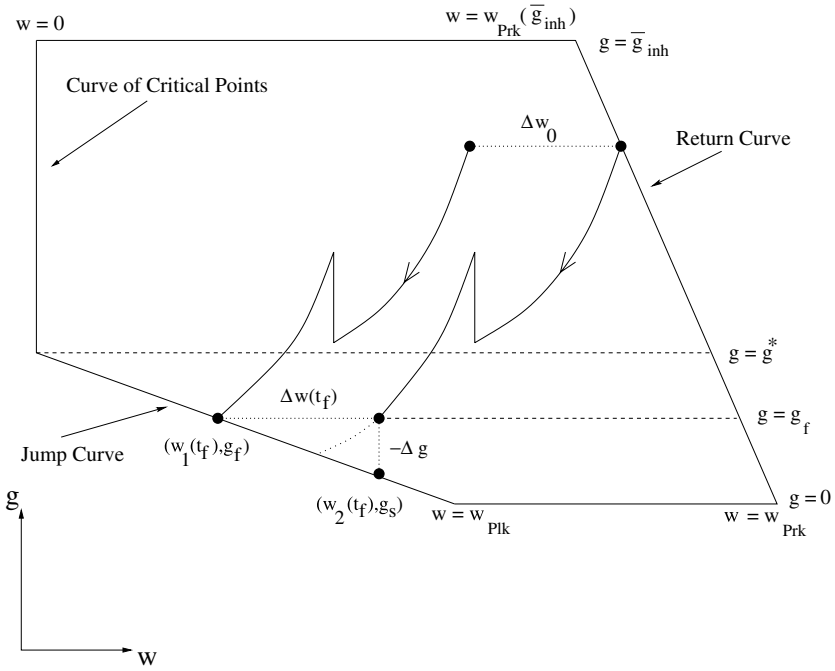

Figure 10. Understanding the basin of attraction. The figure shows important quantities that enter into determining whether or not two initial conditions will synchronize. For clarity, the figure depicts the situation where the cells only receive one bout of inhibition during the silent state. Δw_0 is the initial w distance between the two cells and $\Delta w(t_f)$ is the w distance at time t_f when the leading cell reaches the jump curve. The time Δt in equation (18) is the time to evolve on the dotted vertical line over the distance $-\Delta g$. Since the trailing cell reaches the jump curve at a larger value of g than g_s, its time to the jump curve is less than Δt.

interested in calculating the additional time it takes the trailing cell to reach the jump curve. If this time is less than τ_d, the trailing cell will be able to fire prior to being inhibited resulting in the two cells being more synchronized than when they began. We can compute an upper bound for this time. Use **(A6)** to assume that the slope of the jump curve is given by $-M$. Let $(w_2(t_f), g_s)$ denote the point on the jump curve where the vertical line $w = w_2(t_f)$ intersects it. Let Δt satisfy $g_s = g_f \exp(-\Delta t/\tau_k)$. The time Δt is an upper bound for how long the trailing cell needs to reach the jump curve. It is an upper bound because it assumes that the w variable for the trailing cell does not change. Since this value does change, the trailing cell will actually reach the jump curve with $g > g_s$, and the time of evolution from g_f to that point will be less than Δt. Let $\Delta g = g_s - g_f$. Then $\Delta g = -M\Delta w$. This implies

$$g_f(\mathrm{e}^{-\Delta t/\tau_k} - 1) = -M\Delta w_0 \mathrm{e}^{-t_f/\tau_w}. \tag{17}$$

Solving for Δt, we obtain

$$\Delta t = \tau_k \ln \frac{g_f}{g_f - M\Delta w_0 \mathrm{e}^{-t_f/\tau_w}}. \tag{18}$$

Thus if $\Delta t < \tau_d$, the trailing cell will reach the jump curve before the inhibition from the leading cell affects it. Therefore

$$\tau_k \ln \frac{g_f}{g_f - M\Delta w_0 \mathrm{e}^{-t_f/\tau_w}} < \tau_d, \tag{19}$$

or alternatively

$$\Delta w_0 < \frac{g_f e^{t_f/\tau_w}}{M}(1 - e^{-\tau_d/\tau_k}) \tag{20}$$

provides a condition which when satisfied allows the P cells to synchronize. Note that if $\tau_d = 0$ then (19) or (20) can never be satisfied. This implies that a synaptic delay is a necessary condition to obtain synchrony. Larger values of τ_d clearly allow larger initial differences in w values to synchronize, assuming other quantities in (20) are fixed. The most important way to increase the basin of attraction of the synchronous solution is to increase t_f since the right-hand side of (20) grows exponentially with it.

Let us now consider a few different cases in more detail. Suppose $T_{\text{in}} < T_*$ is small so that I fires frequently and its synapse to the P cell is depressed. Consequently, g_f is small. As $T_{\text{in}} \to 0$, $g_f \to 0$. So (20) can never be satisfied. Thus for high-frequency inhibition, the basin of attraction of the synchronous solution is small. If $T_{\text{in}} > T^*$ is large but fixed, then t_f is bounded from above and is mostly determined by τ_k, and g_f is always bounded above by g^*. Therefore Δw_0 is bounded from above. Finally, consider the case where we ramp the frequency of I. In that case, we can make t_f arbitrarily large by keeping $T_{\text{in}} \in [T_*, T^*]$ for arbitrarily long amounts of time, since the P cells are suppressed in this range. Thus arbitrarily large differences in initial conditions can be overcome if t_f is large enough. The synchronization mechanism is illustrated in the w–g phase plane in figure 11 and in the v–t plane in figure 4.

5. Computational exploration

The synchronization mechanism explained and analysed in section 4 was shown to computationally exist within the PIP network, as demonstrated by figures 2–4. Those simulations used specific parameter values, as detailed in appendix B. In this section, we vary pertinent parameter values to determine their effects on two important characteristics of the system. All of the following simulations used the same initial conditions as those of figure 4. Simulations were done using the differential equation solver XPP [7].

One of the attributes studied is time to first pyramidal cell spike as the system receives SPW input. This time was measured in reference to the SPW input to the interneuron. As explained in appendix B, the simulated SPW starts at $t = 400$ ms. When either of the pyramidal cells fired after 400 ms, its firing time was recorded when its voltage crossed 0 mV. This time was then subtracted from 400 ms to determine the time of the first pyramidal cell action potential. Each time value was rounded to one decimal place. For these simulations, we are primarily interested in whether the pyramidal cells spike within 120 ms of the start of the SPW input, since SPWs rarely last more than that amount of time.

The second characteristic studied is the amount of synchronization between the pyramidal cells during the first spike recorded after the SPW input begins. This was accomplished by measuring the time difference between the pyramidal cell spikes after each has fired for the first time during the SPW. Each time difference was rounded to one decimal place to account for a simulation step size of 0.05 ms. Here, we define synchronization to take place if the cells are within 1 ms of each other. All simulations started with the pyramidal cells 44 ms apart, oscillating out of phase.

The time to first spike is directly related to the time t_f defined in calculations for the basin of attraction from section 4.3. Once the SPW begins, the pyramidal cells are suppressed, preventing them from reaching the jump curve until the synapse is sufficiently depressed. This suppression affects the time for which the leading cell reaches the jump curve, t_f. Equation (20)

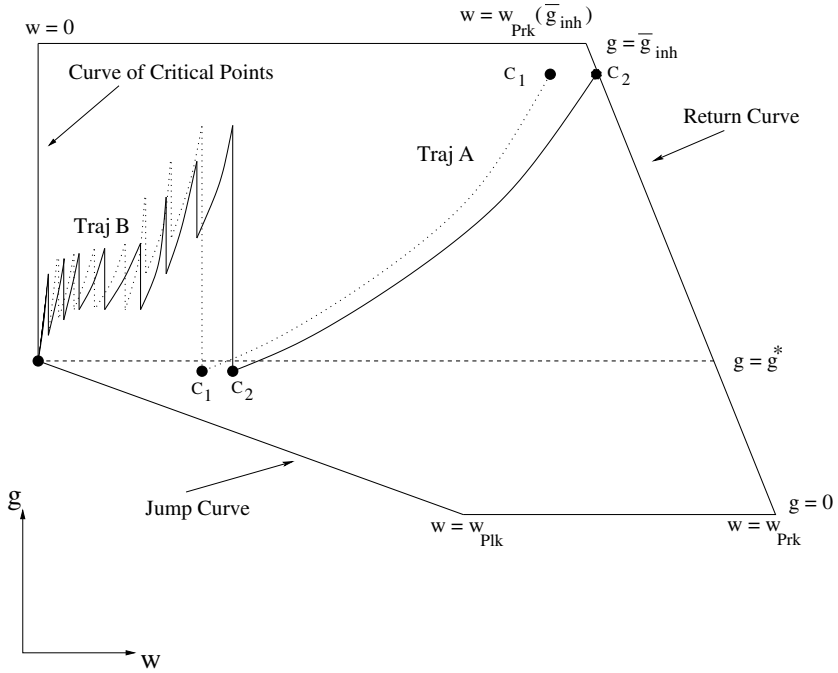

Figure 11. The synchronization mechanism in the w–g phase plane. Both cells start along the same g-level. P cell 1 (dotted trajectory) is ahead of P cell 2 (solid trajectory), where P cell 2 has just returned from the active state. Both cells start in the regime for low-frequency inhibition, causing the I to fire when they fire, as shown in figure 9, Trajectory A. At some time, the inhibition frequency begins to ramp up, as observed during the SPWR, and the P cells approach each other, as they follow a trajectory like Trajectory B in figure 9. Finally, as the synapse depresses, the cells can reach g^* and fire synchronously.

demonstrates that if t_f is increased, the basin of attraction increases. Therefore, we would expect to see an increase in the amount of synchronization. Note that by continuous dependence on initial conditions, greater amounts of synchrony imply a larger basin of attraction for the synchronous solution. In other words, if the time to first spike is increasing, the amount of synchronization and the basin of attraction of the synchronous solution should also increase. Data from all four simulation studies showed this trend.

5.1. Maximum inhibitory frequency

The maximum inhibitory frequency is determined by the average frequency achieved by the interneuron after receiving the ramp input. In the simulations, the frequency was varied by changing the maximum amount of input received when the ramp input was at its maximum value. Figure 12 shows the simulation results.

Increasing the maximum frequency advances the first pyramidal cell spike time. For frequencies less than 140 Hz, the first spike time was greater than 120 ms, the maximal time length of a SPW ripple. And, as is evident in figure 3, for which the frequency was ∼23 Hz, if the maximum frequency gets too small, the interneuron produces no apparent synchronization to record a first spike time. The advance of the first pyramidal cell spike time with increasing frequency is sensible for a given rate of input into the interneuron since the synapse will depress more rapidly and the cells will have a greater chance of reaching g^* in the w–g phase plane earlier between inhibitions.

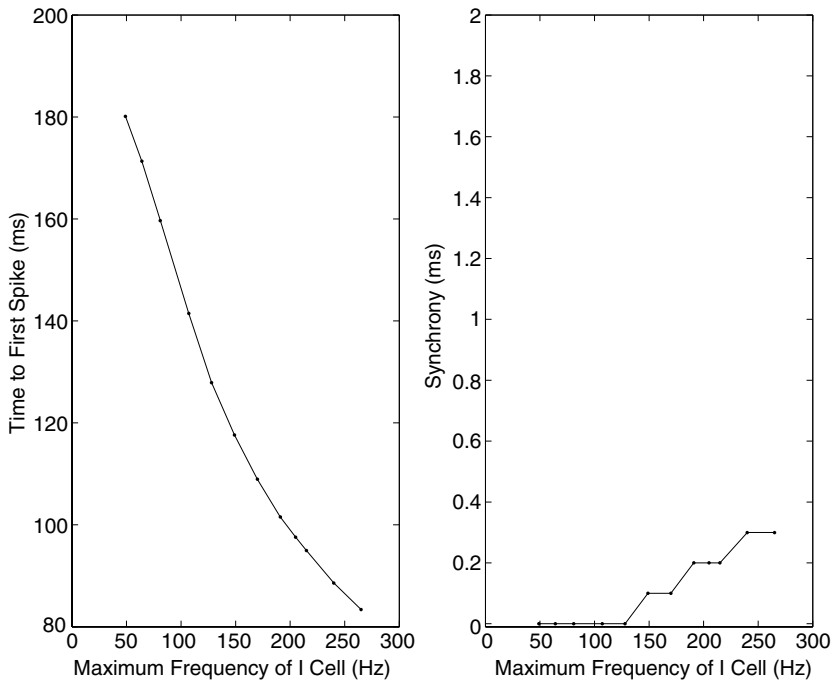

Figure 12. The effects of maximum inhibitory frequency on first time to spike and pyramidal cell synchronization. Increasing the maximum inhibitory frequency advances the first pyramidal cell spike time, and causes a minor drop in synchronization. However, synchronization remained within 1 ms. The control frequency is 205 Hz.

For all choices of maximum frequency, synchronization was well within tolerance. However, there was a marked decrease in synchronization for higher frequencies. Again, this is sensible since an increase in frequency over the same ramp rate will depress the synapse more rapidly over the same amount of time, causing the synapse's synchronization properties to fade more rapidly before suitably synchronizing the pyramidal cells.

5.2. Rate of ramp input to the interneuron

The rate of input to the interneuron in the simulations is determined by the slope of the piecewise linear function described in appendix B. Figure 13 summarizes the results of varying this slope. For each simulation, the simulated SPW began at $t = 400$ ms.

Increasing the rate at which the SPW impinges of the interneuron advances the first pyramidal cell spike. The results here are not surprising. This is similar to increasing the frequency over the same ramp rate. The frequency increases more rapidly and the synapse depresses more quickly, allowing the pyramidal cell to fire earlier. In this parameter regime, the slope needed to be greater than 0.01 in order to have the pyramidal cells spike within 120 ms. A minimum time to fire is indicated by the results, as the slope approaches an instantaneous rise rate. For large values of input slope (not shown in figure 13), the time to first spike approached $\sim$88 ms.

The pyramidal cells remained within 1 ms of each other as the ramp rate was increased. However, there was a slight decrease in synchrony as the ramp rate increased. Again, the more rapid increase in frequency depressed the synapse more quickly, before the pyramidal cells were sufficiently synchronized.

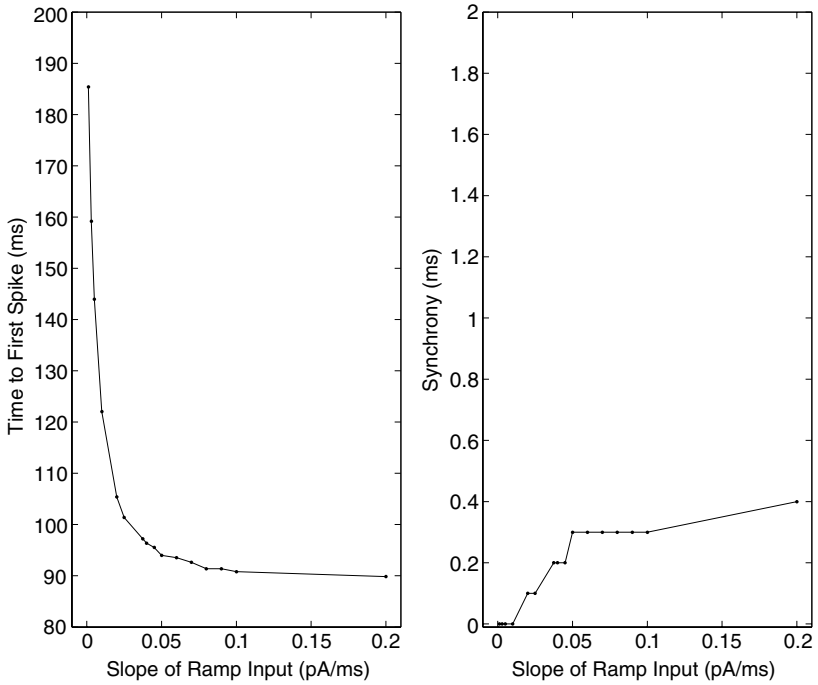

Figure 13. The effects of sharp wave rate of excitation on first time to spike and pyramidal cell synchronization. Increasing the rate advances the first pyramidal cell spike. Increasing the ramp rate caused a minor decrease in synchronization. However, synchronization remains within 1 ms. The control rate is 0.035 pA ms^{-1}.

In vivo, this rate of input depends on multiple factors, such as the number of CA3 pyramidal cells participating in the SPW and the number of synaptic collaterals exciting the interneuron, which may constrain the choice of the rate.

5.3. Inhibitory synaptic decay

The inhibitory synaptic decay time constant is given by the parameter τ_k in the model. Figure 14 displays the simulation results.

Increasing the synaptic decay time constant (which slows the decay rate), delays the first pyramidal cell spike. These results are not surprising since a longer synaptic delay prevents the pyramidal cells from escaping inhibition at an earlier time. All choices of synaptic decay time constants produced a first spike within 120 ms, the typical maximum lifetime of a SPWR.

Synchronization of the pyramidal cells is enhanced by the increase of the synaptic delay time constant. Greater time of decay allows more time for the pyramidal cells to approach each other in the w–g phase plane. Thus, when they fire, they are closer together in time. However, in this parameter regime, the synaptic decay constant needed to be greater than 6 ms in order to produce acceptable synchronization. For these lower values, the τ_k was an order lower than τ_w, allowing a faster decay of inhibition, which allowed the cells to reach the jump curve in the w–g phase plane before having the opportunity to become trapped by the curve of critical points where synchronization could occur.

5.4. Inhibitory synaptic recovery

The time constant for inhibitory synaptic recovery is given by τ_a in the model. Figure 15 depicts this study's findings.

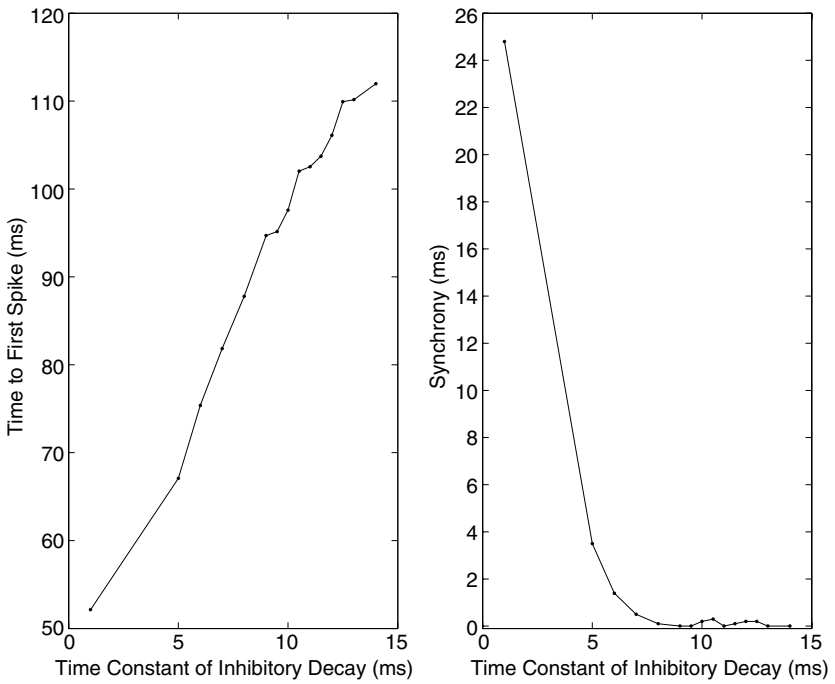

Figure 14. The effects of inhibitory synaptic decay time constant on first time to spike and pyramidal cell synchronization. Increasing the decay time constant (slowing the decay rate) delays the first pyramidal cell spike. However, increasing the time constant also improves synchronization of the pyramidal cells. The control value is $\tau_k = 10$ ms.

Increasing the inhibitory synaptic recovery time constant (which slows its recovery) advanced the first pyramidal cell spike. This result is natural since a slow synaptic recovery increases the inhibitory synaptic depression, allowing the pyramidal cells to fire earlier. For values of τ_a less than 2000 ms, the first spike time was greater than 120 ms. Therefore, the recovery rate must be sufficiently slow to produce a spike within the time interval of a ripple.

Pyramidal cell synchronization decreased as the recovery time constant increased, though for all choices the synchronization was within tolerance. This minor loss of synchrony is not surprising since less recovery produces a weaker synapse and the inhibition is less effective at causing synchronization.

Note that the size of τ_a is very large. This is a result of two factors: (1) the interneuron spends very little time in the active phase, when depression occurs; to offset this very small amount of depression, the recovery needs to very slow, and (2) as discussed in appendix A, τ_a needs to be large enough relative to τ_k in order to ensure the uniqueness of $T_{\max}$, seen in figure 8.

6. Discussion

The main objective of this work is to propose a neural mechanism that may explain why pyramidal cells in CA1 synchronize their firing times during the SPWR [2, 26]. We have shown that ramping up the frequency of an inhibitory interneuron, as observed during actual ripples, can cause pyramidal cells to synchronize in a short amount of time. The key to allowing this synchronization is the role of synaptic depression. Synaptic depression has been found

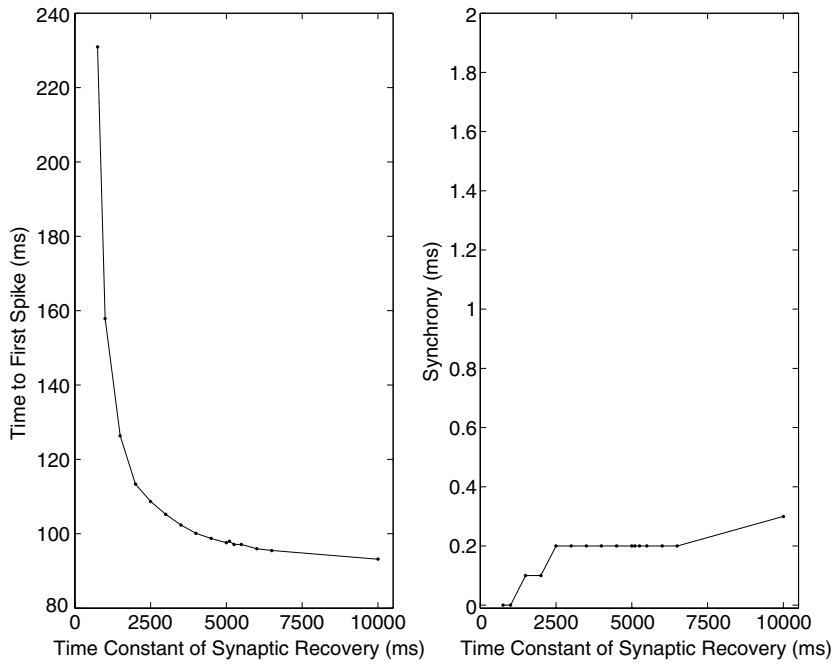

Figure 15. The effects of inhibitory synaptic recovery time constant on first time to spike and pyramidal cell synchronization. Increasing the time constant of inhibitory synaptic recovery (slowing the recovery) advances the first pyramidal spike during the SPWR. Decreasing the recovery rate caused a minor loss of synchronization between the pyramidal cells. However, synchronization remains within 1 ms. The control value of $\tau_a = 5000$ ms.

in inhibitory synapses of CA1 in several experimental studies of both rabbit [20] and rat [16]. Depression allows the pyramidal cells to feel different levels of inhibition at different times, depending on the frequency of I. In particular, depression allows there to be one range of I frequencies which suppresses the firing of pyramidal cells and another at higher frequencies which allows the pyramidal cells to escape the inhibition and fire. We showed that when these two effects are sequentially expressed, i.e. suppression followed by escape, the pyramidal cells synchronize. A primary advantage of this mechanism is that it is completely controlled by the neuronal network. We did not change any parameters associated with the synapse to achieve synchronization, but instead used the physiologically plausible increase in interneuron frequency to foster synchrony.

Our model captures other aspects of the SPWR event. Experimental evidence [4] demonstrates that during SPWRs, interneuron firing probabilities more than double during the preceding 50 ms of the SPWR peak, pointing to a rapid increase of input to the interneurons preceding the SPWR. We have also proposed that the interneurons fire before the pyramidal cell, chiefly due to a period of suppression. The same paper also cites that interneurons discharge before pyramidal cells.

Some aspects of our analysis and simulations were purposely exaggerated to make important points. For example, we use the fact that the inhibition decays slowly when I is below threshold. However, in our simulations we use a time constant of 10 ms for τ_k, which is not overly large. Indeed, it is important that τ_k be of the order of the intrinsic parameter τ_w (15 ms in the simulations) which is the time constant governing the evolution of each P in its silent state. A decay time constant of 10 ms is consistent with that of a GABA-A-mediated

inhibitory current which is widely found in CA1 [8]. Additionally, in figure 8, we show a fairly broad interval $[T_*, T^*]$ in which the maximum of $g_{\min} - g*$ is large. In practice, to achieve synchronization, it is not necessary for this interval $[T_*, T^*]$ to be big, nor need the maximum of $g_{\min} - g^*$ be large. Slowly decaying inhibition will always provide a compression mechanism for synchronization. The size of the basin of attraction of the synchronous solution will depend on the magnitude $g_{\min} - g^*$, together with the manner in which T_{in} is changed. Having said that, ramping the frequency of I will still provide a larger basin of attraction than if the inhibition frequency were kept constant.

In section 4.2, we argued that assumptions **(A1)** and **(A2)** remove any possible time expansions between cells on the jump down to the silent state. Without these assumptions, depending on the slopes of the jump and return curves, it is possible that the synchronous solution is unstable. However, if the time in the active state is bounded, then the amount of time expansion between cells is bounded. Alternatively, our analysis shows that there can be arbitrarily large amounts of time compression in the silent state since the time t_f can be made arbitrarily large by an appropriate ramp in I frequency. Thus, even in the event that the synchronous solution is unstable, the mechanism proposed here implies that the first set of spikes after the ramp can be forced to lie arbitrarily close together in time.

The interval $[T_*, T^*]$ is directly affected by the shape of the $g_{\min} - g^*$ curve, which is determined by several parameters, seen in (14). An obvious way to increase the region of suppression (an increase the amount of synchronization) is to raise the $g_{\min} - g^*$ curve by either by decreasing g^* (requiring the synaptic strength to decay even further before the P cells can fire) or increasing the maximum synaptic strength $\bar{g}_{\text{inh}}$. More subtly, increasing τ_k will have the overall effect of increasing the suppression interval, i.e. slower synaptic decay will increase the time P cells spend in the silent phase, where they are more likely to receive inhibition before reaching the jump curve, as evidenced by figure 14. Even more subtly, if τ_a decreases, the suppression region increases, as demonstrated in figure 15. Since the inhibitory synapse recovers its resources faster, the synapse's strength during successive inhibitions is stronger, leading to the same effect as if the maximum synaptic strength was just increased. A similar effect will occur if τ_b is increased.

Several aspects of this proposed synchronization mechanism are generalizable. For example, there is no difficulty in extending the results to larger globally inhibitory networks consisting of n pyramidal cells. In the paper by Rubin and Terman [18], the existence of N stable clustered states among globally inhibitory networks of excitatory cells was proven. They assumed that the time to reach threshold, and the time for both excitatory cells and interneurons in the active state were constant. By relaxing these conditions, they also showed the existence and stability of two-cluster solutions. Our work shows that within networks of n cells, synchronization will occur in exactly the same way as the two-cell case, again provided that the depression causes there to be a window of suppression.

Heterogeneity between pyramidal cells can also be handled by this mechanism. If each P cell has a slightly different intrinsic frequency, then one can imagine a network of nP cells breaking up into a number of clusters. However, if the depression creates an interval of suppression, then the effect of the heterogeneity will be mitigated. In particular, as the frequency of I is ramped through the interval of suppression and becomes high enough to allow firing, the pyramidal cells could all have been compressed close enough to threshold to disallow the effect of heterogeneity to break up the synchrony. Of course, heterogeneity may only allow the synchrony to last transiently for a few cycles of P firing, but this could be long enough to encompass the length of the ripple. Again, this type of result is very dependent on the degree of heterogeneity, the manner in which the frequency of I is ramped and the parameters $\bar{g}_{\text{inh}}$ and τ_k.

An interesting network effect is the presence of $T_{\max}$. In a previous work [12], a similar network, without excitatory feedback was studied. The value $T_{\max}$ was not present since the P cells had no effect on their mutual inhibitor, the I cell. While the suppression region was still present, the I cell was free to oscillate at any frequency. Here, the frequency of I is constrained from below by the intrinsic frequencies of the P cells, which limits the behaviour of the network. As another example of the impact of the excitatory feedback, $T_{\max}$ could be low enough such that $g_{\min} - g^* < 0$ for all T_{in}. In this case, the P cells fire sufficiently faster than the I cell, causing significant depression, and allowing the P cells to fire with impunity. Ramping I frequency would not have the same synchronizing effect as it does in the case considered in this paper. In short, our results show that the intrinsic properties of P and I cells must work together with properties of the depressing synapses to promote certain types of behaviours such as synchronization or clustering. Our work suggests ways to attain various network behaviours and mechanisms responsible for the transitions between them.

Our model does not directly address the mechanism whereby the SPWR terminates, nor does it discuss the activity of CA1 between SPWs. In practice, the most dominant reason for the end of the ripple may simply be because the SPW input itself ends. Alternatively, it may be that the SPWR ends prior to the end of SPW input, thereby pointing to some neuronal mechanism within CA1 that is responsible for its termination. In different contexts, it has been shown that synchronization can destroy sustained activity [10, 19]. It is unclear, however, in the present context and for our simple model how synchronization could act as a turn-off switch.

The asynchronous behaviour of pyramidal cells between SPW events can be accounted for by our model. Experimental data [4] show that the decay of interneuron firing rates during the tail-end of the SPW is slower than that of the pyramidal cells. In our model, this lingering inhibition would gain strength as the synapses recover, driving apart the pyramidal cells whose synchrony may not have been perfect due to noise or cell heterogeneities. Just as an increase in firing rates can synchronize cells, a decrease in these same rates could desynchronize them.

Acknowledgments

We thank Gyorgy Buzsaki for many helpful discussions which spurred our initial interest in this problem and shaped our approach to it. We also thank the referees for valuable comments and suggestions which helped improve this paper. This research was supported by a grant from the National Science Foundation (DMS-9973230) and by the Burroughs-Wellcome Fund (no 1001749).

Appendix A. Derivation of g_{peak}, $g_{\min}$ and $T_{\max}$

The derivations of g_{peak} and $g_{\min}$ are straightforward. We first solved (7) with $D(0) = D_0$ and (8) with $D(T_{\text{spike}}) = D_0 \exp(-T_{\text{spike}}/\tau_b)$. Next we enforced the steady-state condition $D(T_{\text{spike}} + T_{\text{in}}) = D_0$. The value $g_{\text{peak}} = \bar{g}_{\text{syn}} D_0$. The value $g_{\min}$ is obtained by using that $g \equiv \bar{g}_{\text{syn}} D$ when I is active and obeys $g' = -g/\tau_k$ when it is silent.

To establish the existence and uniqueness of the value $T_{\max}$ consider the jump curve along the slow w–g manifold. Using **(A6)**, we assume it is linear and given by the equation $g - g^* = -M(w - w^*)$, where g^* is the minimum inhibitory conductance needed to produce a fixed point on the slow manifold, w^* is the corresponding w value and $M > 0$. By assumption **(A4)**, $w^* = 0$. When there is no inhibition present, $g = 0$ and $w = w_{p_{lk}}$. Therefore the slope of the jump curve is given by $-M = -g^*/w_{p_{lk}}$.

When P returns to the silent state it will do so along the return curve at a point $(w_{p_{rk}}(g_{\text{peak}}), g_{\text{peak}}\exp(-T_{\text{spike}}/\tau_b))$, where g_{peak} is a function of T_{in}. The function $w_{p_{rk}}(g_{\text{peak}})$ is a decreasing function of g, since the cell will return from the active state at a lower value of w if the synaptic inhibition is higher. Let T_p denote the amount of time that P takes to evolve from the return curve to the jump curve. The functions g and w are given by $g = g_{\text{peak}}\exp(-T_{\text{spike}}/\tau_b)\exp(-T_p/\tau_k)$ and $w = w_{p_{rk}}(g_{\text{peak}})\exp(-T_p/\tau_w)$. Substituting these formulae above into the equation for the jump curve, we obtain

$$g_{\text{peak}}\mathrm{e}^{-\frac{T_{\text{spike}}}{\tau_b}}\mathrm{e}^{-\frac{T_p}{\tau_k}} + \frac{g^* w_{p_{rk}}(g_{\text{peak}})}{w_{p_{lk}}}\mathrm{e}^{-\frac{T_p}{\tau_w}} = g^*. \tag{A.1}$$

Consider the following function of T_{in}:

$$J(T_{\text{in}}) = g_{\text{peak}}\mathrm{e}^{-\frac{T_{\text{spike}}}{\tau_b}}\mathrm{e}^{-\frac{T_{\text{in}}}{\tau_k}} + \frac{g^* w_{p_{rk}}(g_{\text{peak}})}{w_{p_{lk}}}\mathrm{e}^{-\frac{T_{\text{in}}}{\tau_w}} - g^*. \tag{A.2}$$

A zero of the function $J(T_{\text{in}})$ corresponds to a situation where the pyramidal cell spends exactly T_{in} amount of time in the silent state. In other words, a zero of J corresponds to the situation where the amount of time I spends in the silent state switches from being controlled by T_{in} to being controlled by P. Consider (A.2) with $T_{\text{in}} = 0$. Then $J(0) = g^*((w_{p_{rk}}(0)/w_{p_{lk}}) - 1) > 0$ since $g_{\text{peak}} = 0$ when $T_{\text{in}} = 0$ and $w_{p_{rk}}(0) \geqslant w_{p_{rk}}(g_{\text{peak}}) > w_{p_{lk}}$. Alternatively, (A.2) with $T_{\text{in}} \to \infty$ implies that $J(T_{\text{in}}) \to -g^* < 0$, since g_{peak} is bounded by $\bar{g}_{\text{inh}}$, as implied by (13). Thus, the intermediate value theorem implies that there exists a value $T_{\max}$ at which $J(T_{\max}) = 0$. To show uniqueness of this value observe that

$$\frac{\mathrm{d}J}{\mathrm{d}T_{\text{in}}} = \left(\frac{\mathrm{d}g_{\text{peak}}}{\mathrm{d}T_{\text{in}}} - \frac{g_{\text{peak}}}{\tau_k}\right)\mathrm{e}^{-\frac{T_{\text{spike}}}{\tau_b}}\mathrm{e}^{-\frac{T_{\text{in}}}{\tau_k}} + \left(\frac{\mathrm{d}w_{p_{rk}}}{\mathrm{d}g_{\text{peak}}}\frac{\mathrm{d}g_{\text{peak}}}{\mathrm{d}T_{\text{in}}} - \frac{w_{p_{rk}}}{\tau_w}\right)\frac{g^*}{w_{p_{lk}}}\mathrm{e}^{-\frac{T_{\text{in}}}{\tau_w}}. \tag{A.3}$$

Using (15), the derivative $\mathrm{d}g_{\text{peak}}/\mathrm{d}T_{\text{in}}$ can be made smaller by making τ_a larger, and it is bounded above by $\bar{g}_{\text{inh}}/[\tau_a[1 - \exp(-T_{\text{spike}}/\tau_b)]]$ and $w_{p_{rk}}$ is a decreasing function of g_{peak}. Thus by making τ_a large enough relative to τ_k, we guarantee that $\mathrm{d}J/\mathrm{d}T_{\text{in}} < 0$ for all values of T_{in}. The monotonicity of $J(T_{\text{in}})$ guarantees that $T_{\max}$ is unique.

Appendix B. Full equations and simulation values

The general model used to represent a single, isolated neuron (both excitatory and inhibitory) is a conductance-based Hodgkin–Huxley model for spiking neurons developed by Traub and Miles [24] and reduced to a single compartment by Ermentrout and Kopell [6]: $C\frac{\mathrm{d}v}{\mathrm{d}t} = I_0 - g_L(v - V_L) - g_K w^4(v - V_K) - g_{\text{Na}}m_\infty^3(v)h(w)(v - V_{\text{Na}}) - I_{\text{syn}}$ and $\mathrm{d}w/\mathrm{d}t = (w_\infty(v) - w)/\tau_w(v)$. The differential equation for voltage, v, included an input current, ionic currents for leak, potassium, a sodium and, if a connection exists, a synaptic current, I_{syn}, governed by equations (4)–(8) in section 3.2.

The equation for the activation of the potassium gating variable, w, is defined by $w_\infty(v) = a_w(v)/(a_w(v) + b_w(v))$ and $\tau_w(v) = \tau_w$ while the cell is in the silent phase (as mentioned in assumption **(A4)**) and $\tau_w(v) = \tau_r$ when the cell is in the active phase. The function $a_w(v) = 0.032(v + 52)/(1 - \mathrm{e}^{-\frac{v+52}{5}})$ and $b_w(v) = 0.5\mathrm{e}^{-\frac{57+v}{40}}$.

The steady-state sodium activation curve $m_\infty(v) = a_m(v)/(a_m(v) + b_m(v))$, where $a_m(v) = 0.32(54 + v)/(1 - \mathrm{e}^{-\frac{v+54}{4}})$ and $b_m(v) = 0.28(v + 27)/(\mathrm{e}^{\frac{v+27}{5}} - 1)$. For the inactivation of the sodium channels, $h = \max(1 - 1.25w, 0)$.

The values of the parameters used in the simulations are: $C = 1\ \mu\text{F cm}^{-2}$, $g_{\text{Na}} = 100\ \text{ms cm}^{-2}$, $V_{\text{Na}} = 50\ \text{mV}$, $g_K = 80\ \text{ms cm}^{-2}$, $V_K = -100\ \text{mV}$, $g_L = 0.1\ \text{ms cm}^{-2}$, $V_L = -65.625\ \text{mV}$ for pyramidal cells and $V_L = -64.6\ \text{mV}$ for the interneuron, $\tau_b = 0.9\ \text{ms}$,

$\tau_k = 10$ ms, $\tau_a = 5000$ ms, $\tau_w = 15$ ms and $\tau_r = 0.1$ ms. The time constant τ_g is modelled to be infinitesimally small so that $s = D$ whenever the interneuron crosses its synaptic threshold.

The synaptic parameters are: $g_{i\text{syn}} = 0.75$ ms cm^{-2}, $V_{i\text{syn}} = -80$ mV, $g_{e\text{syn}} = 5$ ms cm^{-2}, $V_{e\text{syn}} = 0$ mV.

The injected current I_0 was varied. For the ramp current used to synchronize the P cells, a piece-wise, linear function was used. For times before $t = 400$ ms, $I_0(t) = 0$. For times $400 \text{ ms} \leqslant t \leqslant 400 + \frac{1}{0.035}$ ms (a time of about 30 ms), the function increased in a linear fashion from 0 to 1, with a slope of 0.035. For times greater than $400 + \frac{1}{0.035}$ ms, $I_0(t) = 1$. The synaptic delay $\tau_d = 1$, but can be varied.

References

[1] Bose A, Manor Y and Nadim F 2001 Bistable oscillations arising from synaptic depression *SIAM J. Appl. Math.* **62** 706–27

[2] Buzsaki G, Horvath Z, Urioste R, Hetke J and Wise K 1992 High-frequency network oscillations in the hippocampus *Science* **256** 1025–7

[3] Christian E P and Dudek F E 1988 Electrophysiological evidence from glutamate microapplications for local excitatory circuits in the CA1 area of the rat hippocampus *J. Neurophysiol.* **59** 110–23

[4] Csicsvari J, Hirase H, Czurko A, Mamiya A and Buzsaki G 1999 Oscillatory coupling of hippocampal pyramidal cells and interneurons in the behaving rat *J. Neurosci.* **15** 30–46

[5] Draguhn A, Traub R D, Schmitz D and Jefferys J G R 1998 Electrical coupling underlies high-frequency oscillations in the hippocampus *in vitro Nature* **394** 189–92

[6] Ermentrout B and Kopell N 1998 Fine structure of neural spiking and synchronization in the presence of conduction delays *Proc. Natl Acad. Sci. USA* **95** 1259–64

[7] Ermentrout B 2002 *Simulating, Analyzing, and Animating Dynamical Systems: A Guide to XPPAUT for Researchers and Students* (Philadelphia, PA: SIAM)

[8] Freund T and Buzsaki G 1996 Interneurons in the hippocampus *Hippocampus* **6** 345–470

[9] Hebb D 1949 *Organization of Behavior* (New York: Wiley)

[10] Laing C and Chow C 2001 Stationary bumps in networks of spiking neurons *Neural Comput.* **13** 1473–94

[11] Kopell N, Ermentrout G B, Whittington M and Traub R 2000 Gamma rhythms and beta rhythms have different synchronization properties *Proc. Natl Acad. Sci.* **97** 1867–72

[12] Kunec S 2002 Temporal synchronization of CA1 pyramidal cells by high-frequency, depressing inhibition, in the presence of intracellular noise *Doctoral Dissertation* New Jersey Institute of Technology

[13] Mishchenko M and Rozov N 1980 *Differential Equations with a Small Parameter and Relaxation Oscillations* (New York: Plenum)

[14] Morris C and Lecar H 1981 Voltage oscillations in the barnacle giant muscle fiber *Biophys. J.* **35** 193–213

[15] Nadim F, Manor Y, Nusbaum M and Marder E 1998 Frequency regulation of a slow rhythm by a fast periodic input *J. Neurosci.* **18** 5053–67

[16] Nathan T and Lambert J 1991 Depression of fast IPSP underlies paired-pulse facilitation in area CA1 of the rat hippocampus *J. Neurophysiol.* **66** 1704–15

[17] Rubin J and Terman D 2000 Geometric analysis of population rhythms in synaptically coupled neuronal networks *Neural Comput.* **12** 597–645

[18] Rubin J and Terman D 2000 Analysis of clustered firing patterns in synaptically coupled networks of oscillators *J. Math. Biol.* **41** 513–45

[19] Rubin J, Terman D and Chow C 2001 Localized bumps of activity sustained by inhibition in a two-layer thalamic network *J. Comput. Neurosci.* **10** 313–31

[20] Scharfman H and Schwartzkroin P 1989 Selective depression of GABA-mediated IPSP's by somatostatin in area CA1 of rabbit hippocampal slices *Brain Res.* **493** 205–11

[21] Terman D, Bose A and Kopell N 1996 Functional reorganization in thalamocortical networks: transitions between spindling and delta sleep rhythms *Proc. Natl Acad. Sci.* **93** 15417–22

[22] Terman D, Kopell N and Bose A 1998 Dynamics of two mutually coupled slow inhibitory neurons *Physica* D **68** 241–75

[23] Traub R and Bibbig A 2000 A model of high-frequency ripples in the hippocampus based on synaptic coupling plus axon–axon gap junctions between pyramidal neurons *J. Neurosci.* **20** 2086–93

[24] Traub R and Miles R 1991 *Neuronal Networks of the Hippocampus* (Cambridge: Cambridge University Press)

[25] Traub R D, Schmitz D, Jefferys J G R and Draguhn A 1999 High-frequency population oscillations are predicted to occur in hippocampal pyramidal neuronal networks interconnected by axoaxonal gap junctions *Neuroscience* **92** 407–26

[26] Ylinen A, Bragin A, Nasady Z, Jando G, Szabo I, Sik A and Buzsaki G 1995 Sharp wave-associated high-frequency oscillations (200 Hz) in the intact hippocampus: network and intracellular mechanisms *J. Neurosci.* **15** 30–46